

Evaluation of new 2-hydroxy-N-(4-oxo-2-substituted phenyl-1,3-thiazolidin-3-yl)-2-phenylacetamide derivatives as potential antimycobacterial agents

Özlen Güzel-Akdemir^{1,*}, Kübra Demir-Yazıcı¹, Muhammed Trawally¹,
Serap İpek Dingiş-Birgül^{2,3} and Atilla Akdemir²

¹Department of Pharmaceutical Chemistry, Faculty of Pharmacy, Istanbul University, Beyazıt, 34116, Istanbul, Türkiye

²Computer-Aided Drug Discovery Laboratory, Department of Pharmacology, Faculty of Pharmacy, Bezmialem Vakif University, Fatih, 34093, Istanbul, Türkiye

³Department of Pharmaceutical Chemistry, Faculty of Pharmacy, Marmara University, Basibuyuk, 34854, Istanbul, Türkiye

(Received May 13, 2020; Revised May 22, 2020; Accepted May 27, 2020)

Abstract: A small collection of 2-hydroxy-N-(5-methyl/nonsubstituted 4-oxo-2-substituted phenyl-1,3-thiazolidin-3-yl)-2-phenylacetamides (**3-16**) was synthesized from the cyclocondensation of 2-hydroxy-2-phenyl-N'-[(substitutedphenyl)methylene]acetohydrazides (**2**) and mercaptoethanoic acid or 2-mercaptopropanoic acid, characterized with spectral and elemental analysis. In order to explore their antimycobacterial potential, newly synthesized fourteen compounds were screened for their inhibitory activity against *Mycobacterium tuberculosis* strain H37Rv at 6.25 µg/mL with *in-vitro* primary tests. Compound **7** was found to provide the highest inhibition (98%) *M. tuberculosis* strain H37Rv, while most of the new derivatives showed different inhibition ratios. For the search of the putative targets which are considered as related to the antimycobacterial activity of these molecules, docking studies were performed. With molecular dynamic simulations, further possible interactions between ligands and the active site of the selected enzymes were investigated. Eventually, molecular modelling studies indicated that at least part of the mechanism of action of these compounds may be mediated by inhibition of MtInhA.

Keywords: *Mycobacterium tuberculosis*; 2-hydroxy-2-phenylacetohydrazide; mercaptoethanoic acid; 2-mercaptopropanoic acid; 4-oxo-1,3-thiazolidines; molecular modelling. ©2020 ACG Publication. All right reserved.

1. Introduction

Tuberculosis (TB) is an infectious disease caused by the pathogenic bacterium *Mycobacterium tuberculosis* (MT), which spreads through the aerosol droplets contaminated by MT and affects the lungs. TB has a number of symptoms like prolonged cough, chest pain, weakness, weight loss and fever. It is primarily a pulmonary infection but can affect extrapulmonary sites including bones, the central nervous system, and many other organ systems.^{1,2} According to the World Health Organization (WHO) data, TB

* Corresponding author: E-Mail: oguzel@istanbul.edu.tr, Phone: +90 212 455 5700 Ext. 13440

is one of the top 10 causes of death worldwide and a total of 1.5 million people died from TB in 2018. Especially the 30 high TB burden countries like India, China, Indonesia and others accounted for 87% of new TB cases.^{3,4} In addition, studies about the predicted impact of the COVID-19 pandemic on global TB cases and deaths have suggested that TB case detection has decreased by an average of 25% over 3 months (as compared to the level of detection before the pandemic). This would lead to an additional 190 000 (56 000 – 406 000) TB deaths (a 13% increase), bringing the total to 1.66 (1.3 – 2.1) million TB deaths in 2020.⁵

Today, TB is treated by the standard 6 month course of 4 antibiotics. In the standard therapy, a cocktail of first-line drugs isoniazid (INH), rifampin (RIF), pyrazinamide (PZA) and ethambutol (EMB) are given for six months. If the treatment does not reach the success because of bacterial drug resistance, or intolerance to one or more drugs, second-line drugs are used, such as para-amino-salicylate (PAS), kanamycin, fluoroquinolones, capreomycin, ethionamide and cycloserine, which are usually either less effective or more toxic with serious side effects.⁶ Although it is curable, the drug resistance in *M. Tuberculosis* is the major problem as a result of non-adherence to the treatment and chromosomal mutations in Tubercle bacilli that have made them resistant to every drug used to treat tuberculosis.^{7,8}

The *Mycobacterium tuberculosis* enoyl-acyl carrier protein reductase (MtInhA) is an essential enzyme of the type II fatty acid synthase (FAS-II) system, which is the target for well-known first-line antitubercular drug isoniazid (INH) and of the second-line drug ethionamide (ETH).⁹ Mycolic acid, the major component of mycobacterial cell walls, is synthesized through the function of type I (FAS-I) and type II (FAS-II) synthase systems, which utilizes long-chain fatty acids as the raw material. FAS-I system provides the synthesis of fatty acids 16-24 carbons in length and then FAS-II system extends the fatty acid chain, and further to form the mycolic acids.¹⁰ MtInhA catalyzes the NADH-dependent reduction of the double bond of 2-trans-enoyl-[acyl-carrier protein], which is an important step at FAS-II pathway to extend fatty acid chain.¹¹ As a result of inhibition of mycolic acid synthesis, the mycobacterial cell membrane is not able to protect its integrity and survival of the pathogenic bacteria is no more possible. Therefore, inhibition of MtInhA enzyme presents a promising target for new antimycobacterial candidates.

1,3-thiazolidin-4-one derivatives or 4-thiazolidinones namely, exhibit a wide variety of biological properties such as analgesic,¹² antibacterial,¹³ antiparasitic,¹⁴ antioxidant,¹⁵ anticonvulsant,¹⁶ anti-HIV,¹⁷ antifungal,¹⁸ anticancer¹⁹ and in particularly antimycobacterial^{20,21} activities. In our previous study, some 4-thiazolidinone containing compounds were synthesized and evaluated for their human carbonic anhydrase IX (hCA IX) inhibitory activity as potential anticancer agents.²² Again in our very recent work, a different series of 1,3-thiazolidin-4-one derivatives were investigated as inhibitors of fungal carbonic anhydrases of *Candida* spp. and also tested against some Gram-positive and Gram-negative bacteria.²³

In view of the fact that 1,3-thiazolidine ring possesses antimycobacterial activity and as part of our previous studies, in this project, fourteen new 2-hydroxy-*N*-(5-methyl/nonsubstituted 4-oxo-2-substituted phenyl-1,3-thiazolidin-3-yl)-2-phenylacetamide derivatives were synthesized and tested for their antimycobacterial activity against *Mycobacterium tuberculosis* strain H37Rv at 6.25 µg/mL with *in-vitro* primary tests. Subsequently, molecular modelling and dynamic studies were performed to elucidate the interactions between ligands and MtInhA (4BGE), MtInhA (4TZK) and MtInhA (4BQP) active sites, the enzymes which are considered as potentially related to the antimycobacterial activity.

2. Experimental

2.1. Chemical Material and Apparatus

DL 2-hydroxy-2-phenylacetic acid methyl ester, mercaptoacetic acid, 2-mercaptopropionic acid, and aromatic aldehydes were purchased from commercial sources. 2-Hydroxy-2-phenylacetohydrazide (**1**) was synthesized as reported in the literature.²⁴ Uncorrected melting points were recorded using Büchi 530 apparatus and reported in degree centigrade. Leco 932 elemental analyzer was used to conduct elemental analyses. Infrared (IR) spectra were recorded as thin KBr pellets on Perkin Elmer Model 1600 FT-IR spectrophotometer. The values of the frequencies were expressed in cm⁻¹. ¹H-NMR and ¹³C-NMR (APT) measurements were assessed in DMSO-*d*₆ with Varian Inova 500, Bruker DPX 400 MHz instruments. Mass spectra (LC-MS-APCI) were performed in a negative ionization mode on a Finnigan LCQ Mass Spectrometer.

2.2. Chemistry

2.2.1. Synthesis of 2-Hydroxy-2-phenyl-N'-(substituted phenyl)methylene]acetohydrazides (2)

A solution of **1** (0.006 mol) in absolute EtOH (30 mL) was heated with an appropriate aromatic aldehyde (0.0066 mol) under reflux for 4h to give a precipitate which was filtered and purified by either washing it with hot EtOH or recrystallizing it from EtOH to yield the desired product.

2.2.2. General Method for the Synthesis of 2-Hydroxy-N-(4-oxo-2-substitutedphenyl-thiazolidin-3-yl)-2-phenylacetamides (3-8) and 2-Hydroxy-N-(5-methyl-4-oxo-2-substitutedphenyl-thiazolidin-3-yl)-2-phenylacetamides (9-16)

Using a Dean-Stark water separator, a mixture of **2** (0.005 mol) and 2-mercaptopropanoic acid or mercaptoethanoic acid (0.02 mol) was refluxed in dry benzene (30 mL) for 6h. The residue obtained after eliminating the excess of the solvent under reduced pressure was triturated with saturated NaHCO₃ to achieve a complete evolution of CO₂ gas. The resulting crude product was refrigerated overnight, was washed with H₂O, dried and recrystallized from H₂O or EtOH to give the aimed compounds.

N-[2-(4-Bromophenyl)-4-oxo-1,3-thiazolidin-3-yl]-2-hydroxy-2-phenylacetamide (**3**): Yield 7%; m.p. 179 °C. IR (ν, cm⁻¹): 3254 (NH), 1722, 1684 (C=O); ¹H-NMR (500 MHz, δ, ppm): 3.72 (1H, dd, *J*=15.8, 3.1 Hz, thiaz. C₅-H), 3.84 (1H, dd, *J*=15.8, 1.8 Hz, thiaz. C₅-H), 4.94 (1H, d, *J*=4.9 Hz, CHOH), 5.76 (1H, s, thiaz. C₂-H), 6.21, 6.25 (1H, 2d, *J*=5.1 Hz, OH), 7.13-7.26 (5H, m, Ar-H), 7.35 2H, d, *J*=8.8 Hz, Ar-H) 7.48, 7.55 (1H, 2d, *J*=8.3 Hz, Ar-H), 7.55 (1H, d, *J*=8.8 Hz, Ar-H), 10.28, 10.33 (1H, 2s, CONH); ¹³C-NMR [APT (decoupled), 125.6 MHz, δ, ppm]: 29.9 (thiaz. C₅), 61.5 (thiaz. C₂), 73.5 (CH-OH), 127.4, 128.2, 128.6, 130.9, 131.9 (ar. CH), 122.8 (=C-Br), 138.0, 141.0 (ar. =C), 169.2 (amide C=O), 171.5 (thiaz. C=O); MS-APCI (150 eV, *m/z*, %): 407 (43), 405 (M-H, 39), 332 (100), 331 (98), 273 (72), 271 (67), 199 (63), 197 (67). Anal. Calcd. for C₁₇H₁₅BrN₂O₃S (407.28) : C, 50.10; H, 3.71; N, 6.88. Found: C, 50.50; H, 3.71; N, 6.76.

N-[2-(3-Chlorophenyl)-4-oxo-1,3-thiazolidin-3-yl]-2-hydroxy-2-phenylacetamide (**4**): Yield 17%; m.p. 195-196 °C IR (ν, cm⁻¹): 3333 (NH), 1710, 1671 (C=O); ¹H-NMR (500 MHz, δ, ppm): 3.69-3.88 (2H, d, *J*=5.37 Hz, thiaz. C₅-H), 4.95 (1H, s, CHOH), 5.75 (1H, s, thiaz. C₂-H), 6.19 (1H, s, OH), 7.16-7.22 (5H, m, Ar-H), 7.30-7.33 (2H, m, Ar-H), 7.36-7.38 (1H, m, Ar-H), 7.47 (1H, s, Ar-H), 10.35 (1H, s, CONH). Anal. Calcd. for C₁₇H₁₅ClN₂O₃S.½H₂O (371.85): C, 54.51; H, 4.33; N, 7.53. Found: C, 55.17; H, 3.90; N, 7.64.

N-[2-(2,6-Dichlorophenyl)-4-oxo-1,3-thiazolidin-3-yl]-2-hydroxy-2-phenylacetamide (**5**): Yield 32%; m.p. 184 °C. IR (ν, cm⁻¹): 3301 (NH), 1713, 1679 (C=O); ¹H-NMR (500 MHz, δ, ppm): 3.80 (2H, dd, *J*=15.8 Hz, thiaz. C₅-H), 5.00 (1H, s, CHOH), 6.11 (1H, s, thiaz. C₂-H), 6.26 (1H, s, OH), 7.23 (5H, m, Ar-H), 7.40 (1H, d, *J*=8.8 Hz, Ar-H), 7.58 (1H, s, Ar-H), 7.66 (1H, d, *J*=8.3 Hz, Ar-H), 10.47 (1H, s, CONH). Anal. Calcd. for C₁₇H₁₄Cl₂N₂O₃S (397.28): C, 51.40; H, 3.55; N, 7.05. Found: C, 51.19; H, 3.06; N, 6.89

N-[2-(4-Fluorophenyl)-4-oxo-1,3-thiazolidin-3-yl]-2-hydroxy-2-phenylacetamide (**6**): Yield 34%; m.p. 156 °C. IR (ν, cm⁻¹): 3203 (NH), 1713, 1673 (C=O); ¹H-NMR (400 MHz, δ, ppm): 3.69 (1H, dd, *J*=15.6, 1.5 Hz, thiaz. C₅-H), 3.83 (1H, dd, *J*=15.6, 7.4 Hz, thiaz. C₅-H), 4.91 (1H, t, *J*=5.2 Hz, CHOH), 5.75 (1H, s, thiaz. C₂-H), 6.15, 6.20 (1H, 2d, *J*=4.9 Hz, OH), 7.04-7.23 (5H, m, Ar-H), 7.35-7.42 (4H, m, Ar-H), 10.20, 10.24 (1H, 2s, CONH); ¹³C-NMR [APT (decoupled), 125.6 MHz, δ, ppm]: 30.1 (thiaz. C₅), 61.7 (thiaz. C₂), 73.3 (CHOH), 116.0, 127.5, 128.2, 128.6, 130.9 (ar. =CH), 162.0, 164.0 (=C-F), 134.6, 141.0 (ar. =C), 169.1 (amide C=O), 171.3 (thiaz. C=O); MS-APCI (150 eV, *m/z*, %): 345 (M-H, 24), 271 (94), 211 (38), 137 (100). Anal. Calcd. for C₁₇H₁₅FN₂O₃S (346.37): C, 59.00; H, 4.36; N, 8.09. Found: C, 58.40; H, 4.33; N, 7.75.

N-[2-(4-Methoxyphenyl)-4-oxo-1,3-thiazolidin-3-yl]-2-hydroxy-2-phenylacetamide (**7**): Yield 13%; m.p. 174 °C. IR (ν, cm⁻¹): 3332 (NH), 1709, 1673 (C=O); ¹H-NMR (400 MHz, δ, ppm): 3.70 (3H, s, OCH₃),

3.71 (1H, d, $J=16.1$ Hz, thiaz. C₅-H), 3.84 (1H, d, $J=15.4$ Hz, thiaz. C₅-H), 4.96 (1H, s, CHOH), 5.77 (1H, s, thiaz. C₂-H), 6.19 (1H, d, $J=4.4$ Hz, OH), 6.90-6.98 (3H, m, Ar-H), 7.17-7.23 (6H, m, Ar-H), 10.31 (1H, s, CONH); ¹³C-NMR [APT (decoupled), 125.6 MHz, δ , ppm]: 30.1 (thiaz. C₅), 55.7 (OCH₃), 62.3 (thiaz. C₂), 73.3 (CH-OH), 113.2, 115.6, 127.4, 128.1, 128.5, 130.1 (ar. CH), 140.2, 141.1 (ar. =C), 160.1 (=C-OCH₃), 169.4 (amide C=O), 171.4 (thiaz. C=O); MS-APCI (150 eV, m/z , %): 357 (M-H, 9), 283 (46), 223 (19), 149 (100). Anal. Calcd. for C₁₈H₁₈N₂O₄S (358.41): C, 60.3; H, 5.06; N, 7.82. Found: C, 61.10; H, 4.66; N, 7.79.

N-[2-(4-Benzoyloxyphenyl)-4-oxo-1,3-thiazolidin-3-yl]-2-hydroxy-2-phenylacetamide (**8**): Yield 35%; m.p. 162 °C. IR (ν , cm⁻¹): 3360 (OH, NH), 1724, 1691 (C=O); ¹H-NMR (400 MHz, δ , ppm): 3.68 (1H, d, $J=15.3$ Hz, thiaz. C₅-H), 3.81 (1H, dd, $J=15.3, 1.5$ Hz, thiaz. C₅-H), 4.94, 4.95 (1H, 2s, CHOH), 5.11, 5.14 (2H, 2s, OCH₂), 5.73 (1H, s, thiaz. C₂-H), 6.40 (1H, br s, OH), 6.92-7.00 (2H, m, Ar-H), 7.08-7.62 (13H, m, Ar-H), 10.45 (1H, s, CONH). Anal. Calcd. for C₂₄H₂₂N₂O₄S (434.50): C, 66.34; H, 5.10; N, 6.45. Found: C, 66.33; H, 5.05; N, 6.43.

N-[2-(4-Bromophenyl)-5-methyl-4-oxo-1,3-thiazolidin-3-yl]-2-hydroxy-2-phenylacetamide (**9**): Yield 40%; m.p. 210 °C. IR (ν , cm⁻¹): 3238 (OH, NH), 1721, 1685 (C=O); ¹H-NMR (400 MHz, δ , ppm): 1.47 (3H, t, $J=6.3$ Hz, thiaz. C₅-CH₃), 4.01, 4.11 (1H, 2q, $J=6.9$ Hz, thiaz. C₅-H), 4.92 (1H, d, $J=4.7$ Hz, CHOH), 5.73 (1H, s, thiaz. C₂-H), 6.23 (1H, s, OH), 7.14-7.26 (5H, m, Ar-H), 7.34 (2H, d, $J=8.8$ Hz, Ar-H), 7.54 (2H, d, $J=8.4$ Hz, Ar-H), 10.35 (1H, s, CONH). Anal. Calcd. for C₁₈H₁₇BrN₂O₃S (421.31): C, 51.31; H, 4.07; N, 6.65. Found: C, 51.73; H, 4.53; N, 6.66.

N-[2-(3-Chlorophenyl)-5-methyl-4-oxo-1,3-thiazolidin-3-yl]-2-hydroxy-2-phenylacetamide (**10**): Yield 35%; m.p. 187 °C. IR (ν , cm⁻¹): 3241 (OH, NH), 1722, 1682 (C=O); ¹H-NMR (500 MHz, δ , ppm): 1.49, 1.51 (3H, 2d, $J=6.8$ Hz, thiaz. C₅-CH₃), 4.03, 4.12 (1H, 2q, $J=7.0$ Hz, thiaz. C₅-H), 4.95 (1H, d, $J=6.3$ Hz, CHOH), 5.76 (1H, s, thiaz. C₂-H), 6.27 (1H, s, OH), 7.19-7.41 (7H, m, Ar-H), 7.43 (1H, t, $J=8.7$ Hz, Ar-H), 7.50 (1H, d, $J=7.3$ Hz, Ar-H), 10.43 (1H, s, CONH); ¹³C-NMR [APT (decoupled), 125.6 MHz, δ , ppm]: 20.2 (thiaz. CH₃), 39.3 (thiaz. C₅), 55.7 (OCH₃); 60.4 (thiaz. C₂), 73.6 (CH-OH), 127.3, 127.5, 127.6, 128.3, 128.6, 129.7, 130.9, 133.8 (ar. CH), 140.6, 141.0 (ar. =C), 171.7 (amide C=O), 172.3 (thiaz. C=O). Anal. Calcd. for C₁₈H₁₇ClN₂O₃S (376.86): C, 57.37; H, 4.55; N, 7.43. Found: C, 57.33; H, 4.28; N, 7.38.

N-[2-(2,6-Dichlorophenyl)-5-methyl-4-oxo-1,3-thiazolidin-3-yl]-2-hydroxy-2-phenylacetamide (**11**): Yield 24%; m.p. 193-194 °C. IR (ν , cm⁻¹): 3209 (OH, NH), 1722, 1647 (C=O); ¹H-NMR (500 MHz, δ , ppm): 1.48 (3H, q, $J=6.83$ Hz, thiaz. C₅-CH₃), 4.03, 4.13 (1H, 2q, $J=6.83$ Hz, thiaz. C₅-H), 5.10 (1H, s, CHOH), 5.86 (1H, d, $J=5.61$ Hz, thiaz. C₂-H), 6.38 (1H, s, OH), 7.26-7.31 (1H, m, Ar-H), 7.36 (1H, t, $J=7.81$ Hz, Ar-H), 7.41 (2H, t, $J=7.81$ Hz, Ar-H), 7.49 (1H, d, $J=7.81$ Hz, Ar-H), 7.51-7.54 (3H, m, Ar-H), 11.67, 11.78 (1H, 2s, CONH). Anal. Calcd. for C₁₈H₁₆Cl₂N₂O₃S (411.30): C, 52.56; H, 3.92; N, 6.81. Found: C, 54.33; H, 3.21; N, 6.42.

N-[2-(4-Fluorophenyl)-5-methyl-4-oxo-1,3-thiazolidin-3-yl]-2-hydroxy-2-phenylacetamide (**12**): Yield 43%; m.p. 186 °C. IR (ν , cm⁻¹): 3552, 3226 (OH, NH), 1714, 1668 (C=O); ¹H-NMR (400 MHz, δ , ppm): 1.49, 1.50 (3H, 2d, $J=7.0$ Hz, thiaz. C₅-CH₃), 4.03, 4.09 (1H, 2q, $J=6.2$ Hz, thiaz. C₅-H), 4.93 (1H, d, $J=4.3$ Hz, CHOH), 5.76 (1H, s, thiaz. C₂-H), 6.26 (1H, d, $J=4.5$ Hz, OH), 7.17-7.27 (7H, m, Ar-H), 7.42-7.46 (2H, m, Ar-H), 10.36 (1H, s, CONH). Anal. Calcd. for C₁₈H₁₇FN₂O₃S (360.40): C, 59.99; H, 4.75; N, 7.77. Found: C, 59.49; H, 4.97; N, 7.54.

N-[2-(3-Methoxyphenyl)-5-methyl-4-oxo-1,3-thiazolidin-3-yl]-2-hydroxy-2-phenylacetamide (**13**): Yield 18%; m.p. 165 °C. IR (ν , cm⁻¹): 3565, 3212 (OH, NH), 1725, 1688 (C=O); ¹H-NMR (500 MHz, δ , ppm): 1.48 (3H, d, $J=6.83$ Hz, thiaz. C₅-CH₃), 3.77 (3H, s, OCH₃), 3.97, 4.02 (1H, 2q, $J=6.83$ Hz, thiaz. C₅-H), 4.90 (1H, s, CHOH), 5.68 (1H, s, thiaz. C₂-H), 6.19 (1H, s, OH), 6.88-6.90 (2H, m, Ar-H), 7.17-7.21 (1H, m, Ar-H), 7.22-7.26 (4H, m, Ar-H), 7.28 (2H, d, $J=8.79$ Hz, Ar-H), 10.24 (1H, s, CONH). Anal. Calcd. for C₁₉H₂₀N₂O₄S (372.44): C, 61.24; H, 5.41; N, 7.52. Found: C, 60.83; H, 5.40; N, 7.38.

N-[2-(4-Methoxyphenyl)-5-methyl-4-oxo-1,3-thiazolidin-3-yl]-2-hydroxy-2-phenylacetamide (**14**): Yield 16%; m.p. 159 °C. IR (ν, cm⁻¹): 3235 (OH, NH), 1723, 1682 (C=O); ¹H-NMR (500 MHz, δ, ppm): 1.50 (3H, d, *J*=6.8 Hz, thiaz. C₅-CH₃), 3.76 (3H, s, OCH₃), 4.00, 4.07 (1H, 2q, *J*=6.8 Hz, thiaz. C₅-H), 4.94 (1H, d, *J*=3.4 Hz, CHOH), 5.73 (1H, s, thiaz. C₂-H), 6.23 (1H, s, OH), 6.93-7.20 (3H, m, Ar-H), 7.21-7.25 (6H, m, Ar-H), 10.35 (1H, s, CONH). Anal. Calcd. for C₁₉H₂₀N₂O₄S · H₂O (390.40): C, 58.40; H, 5.63; N, 7.17. Found: C, 58.20; H, 4.44; N, 6.96.

N-[2-(3,4-Dimethoxyphenyl)-5-methyl-4-oxo-1,3-thiazolidin-3-yl]-2-hydroxy-2-phenylacetamide (**15**): Yield 20%; m.p. 169-171 °C. IR (ν, cm⁻¹): 3228 (OH, NH), 1722, 1688 (C=O); ¹H-NMR (400 MHz, δ, ppm): 1.48 (3H, d, *J*=4.00 Hz, thiaz. C₅-CH₃), 3.76 (6H, s, 2xOCH₃), 3.98, 4.04 (1H, 2q, *J*=6.97 Hz, thiaz. C₅-H), 4.91 (1H, d, *J*=4.10 Hz, CHOH), 5.70 (1H, d, *J*=7.26 Hz, thiaz. C₂-H); 6.23 (1H, br s., OH), 6.82-6.86 (2H, m, Ar-H), 6.99-7.01 (1H, m, Ar-H), 7.16-7.24 (5H, m, Ar-H), 10.28 (1H, d, *J*=6.37 Hz, CONH). Anal. Calcd. for C₂₀H₂₂N₂O₅S (390.40): C, 59.69; H, 5.51; N, 6.96. Found: C, 59.93; H, 5.50; N, 6.56.

N-[2-(4-Benzyloxyphenyl)-5-methyl-4-oxo-1,3-thiazolidin-3-yl]-2-hydroxy-2-phenylacetamide (**16**): Yield 49%; m.p. 175 °C. IR (ν, cm⁻¹): 3359 (OH, NH), 1724, 1686 (C=O); ¹H-NMR (500 MHz, δ, ppm): 1.46-1.49 (3H, m, thiaz. C₅-CH₃), 3.97, 4.05 (1H, 2q, *J*=6.83 Hz, thiaz. C₅-H), 4.89-4.94 (1H, m, CHOH), 5.09, 5.12 (2H, 2s, OCH₂), 5.68 (1H, t, *J*=6.34 Hz, thiaz. C₂-H), 6.13 (1H, d, *J*=5.37 Hz, OH), 6.91-6.93 (1H, m, Ar-H), 6.96-6.99 (1H, m, Ar-H), 7.14-7.34 (8H, m, Ar-H), 7.39 (2H, t, *J*=6.84 Hz, Ar-H), 7.45-7.47 (2H, m, Ar-H), 10.25 (1H, s, CONH). Anal. Calcd. for C₂₅H₂₄N₂O₄S (448.53): C, 66.94; H, 5.39; N, 6.25. Found: C, 66.98; H, 5.80; N, 6.16.

2.3. Biological Activity

2.3.1. In Vitro Evaluation of Antituberculosis Activity

Using the BACTEC 460 radiometric system, the synthesized compounds were primarily screened for their antituberculosis activity against *Mycobacterium tuberculosis* strain H37Rv at 6.25 µg/mL concentration in BACTEC 12B medium. To determine the actual MIC, only compounds that showed inhibition of at least 90% were chosen for further evaluation in the CABTEC 460 at lower concentrations. The minimum inhibitory concentration (MIC) was defined as the lowest concentration of the compounds that inhibits 99% of the inoculum.²⁵

2.3.2. BACTEC Radiometric Method of Susceptibility Testing

The inocula were drawn from either an isolated positive BACTEC vial for susceptibility testing with a growth index (GI) of at least 500 or from isolates of organisms suspended through a conventional medium. After vigorously mixed with a syringe, inoculum of positive BACTEC culture (0.1 mL) was added to each of the vials containing 6.25 g/mL of the test compounds. For the standard vials, 2.25 g/mL of rifampin (RMP) and a serial dilution of 1:100 of the culture was set for control. In order to provide CO₂ in the headspace, BACTEC instrument was used to test each vial immediately and incubated at 37 °C and monitored daily with BACTEC instrument. A comparison of GI in the control reading at least 30 with that of the drug vial. This was captured as a change in GI to the drug vial. We used the following formula to interpret our results:

$$\begin{aligned} \Delta \text{GI control} > \Delta \text{GI drug} &= \text{susceptible} \\ \Delta \text{GI control} < \Delta \text{GI drug} &= \text{resistant} \end{aligned}$$

A definite pattern of change in GI differences was established based on the additional 1 to 2 days reading of the vials when a clear susceptibility pattern (the difference of change of GI of control and the drug bottle) was not seen when the control GI was 30.

2.4. Molecular Modelling Studies

The MtInhA enzyme was investigated as a possible target for the fourteen thiazolidinone compounds according to the previously described protocol.²⁶

2.4.1. Preparation of Ligands Structures

Three-dimensional structures of all ligands and all their possible stereoisomers were prepared with MOE (v2019.01.02, Chemical Computing Group Inc., Montreal, QC, Canada) in low-energy conformations. The most prevalent protonation state of the ligands at pH 7 was calculated. Finally, the ligands were energy minimized using a steepest-descent protocol MMFF94x force field.²⁷

2.4.2. Preparation of X-ray Structures

The three crystal structures of *Mycobacterium tuberculosis* enoyl-acyl carrier protein reductase (MtInhA) complexed with 1-cyclohexyl-*N*-(3,5-dichlorophenyl)-5-oxopyrrolidine-3-carboxamide (MtInhA; PDB: 4TZK; 1.62 Å), complexed with methyl-thiazole compound (MtInhA; PDB: 4BQP; 1.89 Å) and a mutant (S94A) complexed with pyridomycin (MtInhA(S94A); PDB: 4BGE; 2.25 Å) have been obtained from the RCSB Protein Data Bank. Buffer molecules, ions, and water molecules were deleted, and all other atoms were retained. The remaining structure was protonated according to the protonate 3D protocol found in the MOE package.²⁸ Subsequently, the obtained structures were energy minimized by using the AMBER14:EHT force field.²⁹

2.4.3. Docking Studies

Docking calculations were performed using the FlexX docking tool (v2.3.2; BioSolveIT GmbH, St. Augustin, Germany) within MOE. The binding pockets were defined as all residues within 6.5 Å of the reference ligands 1-cyclohexyl-*N*-(3,5-dichlorophenyl)-5-oxopyrrolidine-3-carboxamide, methyl-thiazole compound and pyridomycin for the crystal structures of MtInhA (PDB:4TZK, 4BQP and 4BGE respectively). All ligands were docked fifty times, and the best-scoring three poses were subjected to refinement calculations. Subsequently, the docked ligand and binding pocket residues were energy-minimized and rescored using the GBVI/WSA force field.³⁰

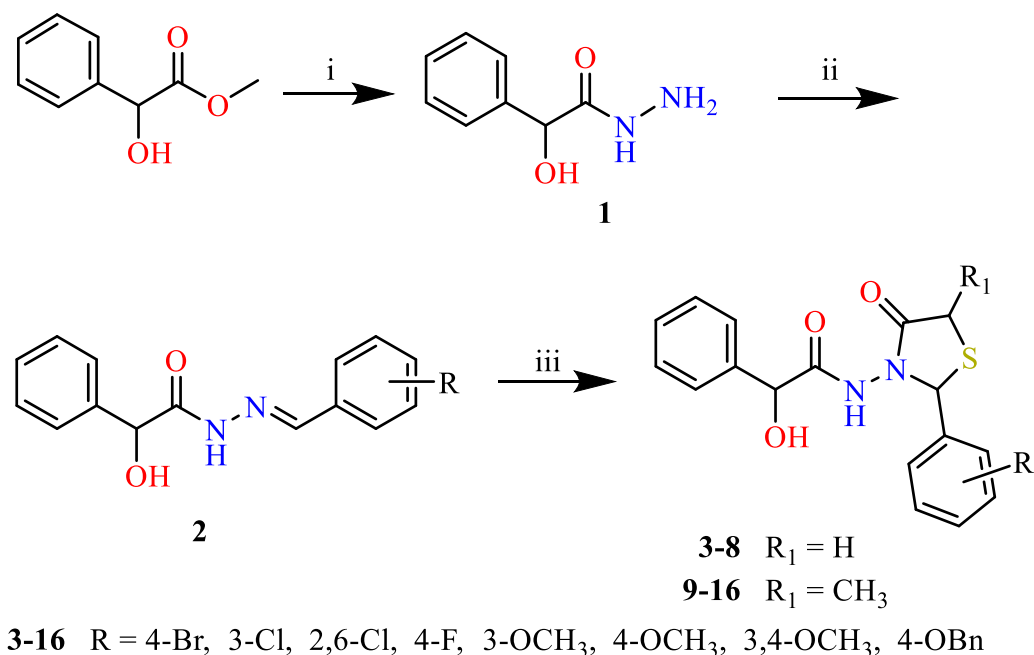
2.4.4. Molecular Dynamics Simulations

By using the NAMD software package (v2.12, Theoretical and Computational Biophysics Group, NIH Center for Macromolecular Modeling and Bioinformatics, The Beckman Institute, University of Illinois at Urbana-Champaign), molecular dynamic (MD) simulations of suggested molecules and original ligands were performed.³¹ The selected docked poses (ligand-enzyme complexes) were first placed into the center of a box with periodic boundary conditions which have a minimum distance of 10 Å between protein and boundary. To create a solvated and neutral system, both water molecules (1.005 g/cm³) and counter ions (NaCl) were added. After the minimization of all structures with a steepest-descent protocol (AMBER14:EHT), the system was first heated from 0 to 300 K for 50 ps followed by a 50 ps equilibration simulation (position restraints on all protein and ligand heavy atoms). Finally, the system was simulated for 2 ns at constant temperature (300 K, Langevin, default values) and pressure (1 bar, Nosé-Hoover Langevin, default values), without any position restraints. The time step was set to 0.002 fs and all bonds were constrained using the ShakeH algorithm.

3. Results and Discussion

3.1. Chemistry

The new thiazolidinone derivatives were prepared from 2-hydroxy-2-phenylacetohydrazide (**1**) obtained from the reaction between DL 2-hydroxy-2-phenylacetic acid methyl ester and hydrazine hydrate. Compound **1** reacted with substituted aromatic aldehydes to afford intermediate Schiff bases (**2**), after that cyclodehydration with mercaptoethanoic acid and 2-mercaptopropanoic acid, targeted compounds, 2-hydroxy-*N*-(4-oxo-2-substitutedphenyl-1,3-thiazolidin-3-yl)-2-phenylacetamides (**3-8**) and 2-hydroxy-*N*-(5-methyl-4-oxo-2-substitutedphenyl-1,3-thiazolidin-3-yl)-2-phenylacetamides (**9-16**) were yielded respectively (Scheme 1).



Scheme 1. Reagents: i) hydrazine hydrate, EtOH, reflux, 6h; ii) EtOH, reflux, 4h; iii) mercaptoethanoic acid / 2-mercaptoopropanoic acid, dry benzene, reflux, 6h

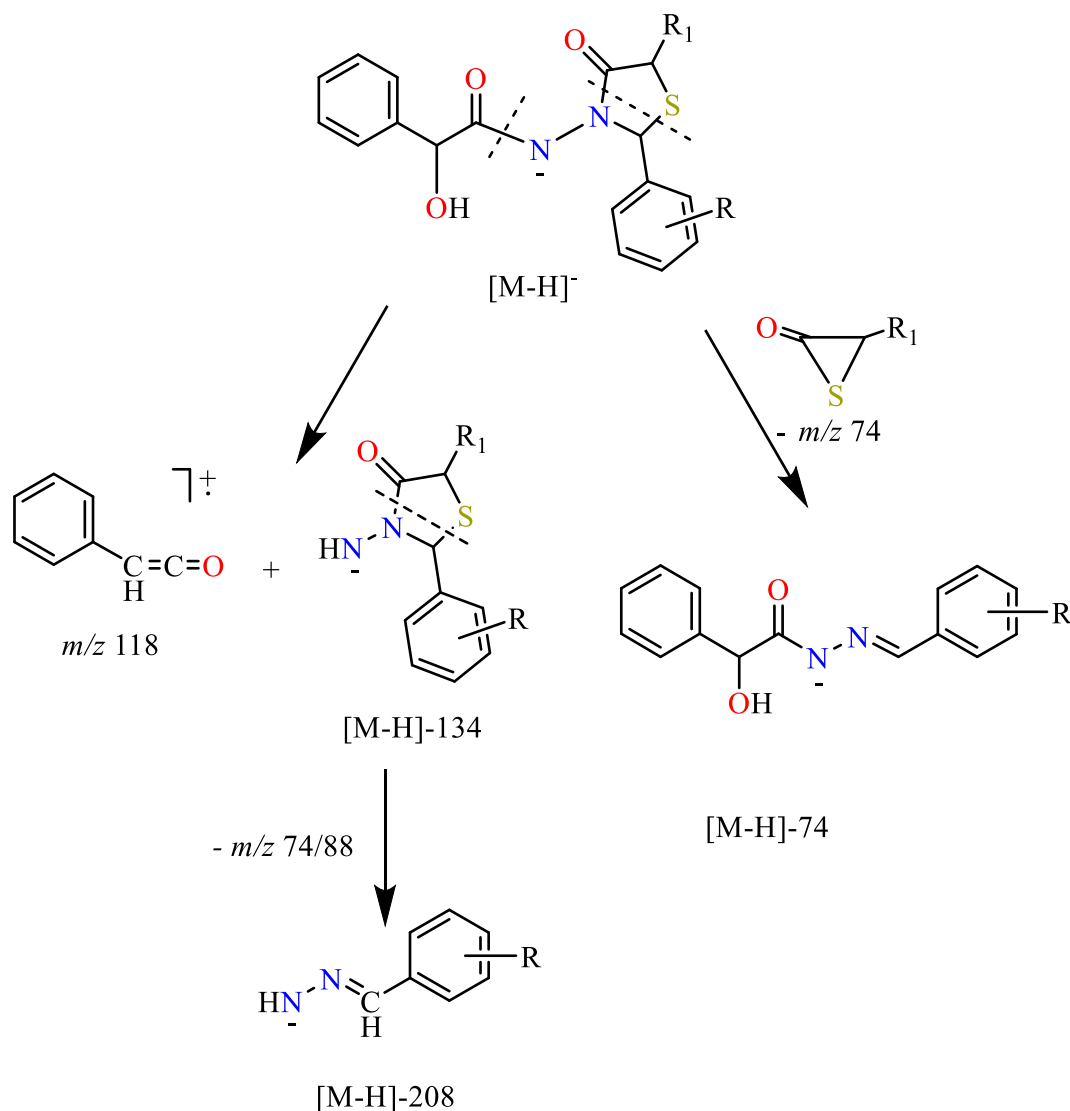
The structures of **3-16** were characterized by elemental analysis and spectral data (IR, ^1H NMR, ^{13}C NMR and APCI Mass).

In the IR spectra of the new compounds, O-H / N-H stretching bands were observed at the 4000–2500 cm^{-1} area between 3209–3565 cm^{-1} . Strong stretching bands of new lactam C=O groups (1709–1725 cm^{-1}) are characteristic for 4-thiazolidinones^{32,33} besides C=O amide bands (1647–1691 cm^{-1}) in the IR spectra confirmed the aimed cyclization of the thiazolidinone ring.³⁴

In the ^1H -NMR spectrums of compounds, the methylene (SCH₂) protons as two singlets or two doublets for compounds **3-8** and methine (SCHCH₃) protons as two quartets for series **9-16** detected at about δ 3.68–3.84 and δ 3.97–4.13 ppm respectively, which are characteristic peaks belong to protons at 5-position of the 2,3 disubstituted 4-thiazolidinone rings.³⁵ The C₂-H protons for all compounds were appeared at about δ 5.68–6.11 ppm. The signals of C-OH and CONH protons were signaled at about δ 6.13–7.44 and δ 10.24–11.78 ppm, respectively. Peaks associated with other protons of the molecules were observed in the expected regions.³⁶

The ^{13}C NMR spectra of **3, 6, 7** and **10** assigned on the basis of APT spectra and literature, showed lactam C=O signals at δ 171.3–172.3 ppm and provided further proof for thiazolidinone formation. C₂ resonances of compounds **3, 6, 7** and **10** appeared at δ 60.40–62.30 ppm. For compounds **3, 6** and **7**, signals of C₅ detected at δ 29.90–30.10 and for compound **10** at δ 39.9 ppm. The chemical shifts of the carbons at aromatic rings observed at the aromatic area, as expected.^{37,38}

(M-H)⁻ ions with different intensities observed in the atmospheric pressure chemical ionization APCI (-) mass spectra of **3, 6** and **7** provided further confirmation for the formation of the expected structures. Compounds **3, 6** and **7** fragmented via two prominent pathways to afford the fragments (M-H)-74 by breaking 1,2 and 3,4 bonds of the thiazolidinone ring and the fragments (M-H)-134 by breaking of the C-N bond the hydrazide moiety. The proposed APCI mass fragmentation route of **3, 6** and **7** recorded employing the negative ionization mode is depicted in Scheme 2.



Scheme 2. Proposed mass fragmentation pattern of compounds **3**, **6** and **7**

3.2. Biological Activity

3.2.1 Antimycobacterial Activity

The selected compounds were evaluated for antituberculosis activity against *Mycobacterium tuberculosis* strain H37Rv. Primary screening was conducted at 6.25 $\mu\text{g}/\text{mL}$ against the microorganism in BACTEC 12B medium using the BACTEC 460 radiometric system. Rifampin was used as the standard in the tests.²⁵ Compounds **3-16** showed varying degrees of inhibition in the primary screen (Table 1).

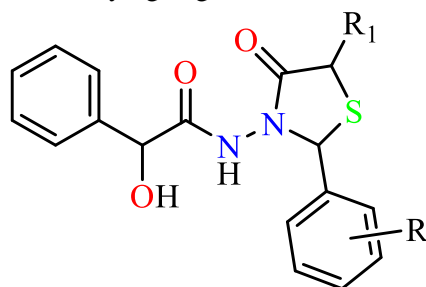


Figure 1. The general chemical structures of novel compounds **3-16**

Table 1. The primary *in vitro* antimycobacterial activity screening results of **3-16**

Compound	R	R ₁	MIC (µg/mL)	Inhibition% ^a
3	4-Br	H	> 6.25	6
4	3-Cl	H	> 6.25	9
5	2,6-Cl	H	> 6.25	31
6	4-F	H	> 6.25	10
7	4-OCH ₃	H	> 6.25	98
8	4-OBn	H	> 6.25	12
9	4-Br	CH ₃	> 6.25	6
10	3-Cl	CH ₃	> 6.25	3
11	2,6-Cl	CH ₃	> 6.25	0
12	4-F	CH ₃	> 6.25	6
13	3-OCH ₃	CH ₃	> 6.25	11
14	4-OCH ₃	CH ₃	> 6.25	0
15	3,4-OCH ₃	CH ₃	> 6.25	22
16	4-OBn	CH ₃	> 6.25	4

^a MIC rifampicin 0.25 µg/mL, 97-99% inhibition versus *M. tuberculosis* strain H37Rv.

As reported in the table above, all the synthesized compounds were tested for their antitubercular activity against *Mycobacterium tuberculosis* strain H37Rv. All the compounds showed antitubercular activity except compounds **11** and **14**. We assessed our SAR based on the modification of substituents of the 5th position and the substituents on the phenyl ring attached to the 2nd position of the thiazolidinone ring.

Except for compound **9**, the addition of a methyl group of position 5 of the thiazolidinone ring yielded a distinct loss of activity against the bacteria. The presence of different substituents on various positions of the phenyl ring resulted in significant changes in the inhibition percentage of the compounds. With regards to the 5-non-methyl thiazolidinone compounds (i.e., compounds **3-8**), the dihalo-substitution of the phenyl ring led to an improvement in the activity when we compared compounds **3**, **4** and **6**. On the contrary, the dihalo-substitution of the phenyl ring in 5-methylthiazolidinone derivatives led to a complete loss of activity (compound **11**).

Replacement of the halogens with a methoxy group on the phenyl ring significantly enhanced the activity. However, the presence of a bulkier group, a benzyloxy group, led to a deterioration in the activity when compounds **7** and **8** are compared. Comparing compounds **13**, **14** and **15**, the dimethoxyphenyl derivative displayed a better antimycobacterial activity than the rest.

3.3. Molecular Modelling Studies

To investigate MtInhA as a possible target for these compounds, we performed molecular modelling studies using the co-crystal structures of this enzyme in complex with 1-cyclohexyl-*N*-(3,5-dichlorophenyl)-5-oxopyrrolidine-3-carboxamide (4TZK), a methyl-thiazole compound (4BQP) and a mutant derivative MtInhA (S94A) complexed with pyridomycin (4BGE). These structures were chosen due to significant differences in the binding pocket. The different rotamers of Tyr158 sidechain at the active site of the MtInhA (4TZK) and (4BQP) affect the ligand's position at the hydrophobic pocket and the possible interactions.³⁹ With a single point mutation allele (S94A) in MtInhA is occurred the single substitution of alanine for serine 94 resulted in INH resistance, which seems to be directly related to decreases the binding affinity of the drug to NAD⁺.^{40,41}

Interesting docked poses have been obtained for the compounds in the active site of MtInhA (4TZK) and MtInhA (4BQP), but not for MtInhA (4BGE).

3.3.1. Docking Studies and MD Simulations into the Active Site of MtInhA (4TZK)

To explain the binding features between the MtInhA (4TZK) crystal structure and the reference ligand 1-cyclohexyl-*N*-(3,5-dichlorophenyl)-5-oxopyrrolidine-3-carboxamide, docking studies and 2 ns MD simulation was performed (Figure 2). In crystal structures of MtInhA (4TZK), NAD⁺ (Nicotinamide Adenine Dinucleotide) is presented as a cofactor of the enzyme.

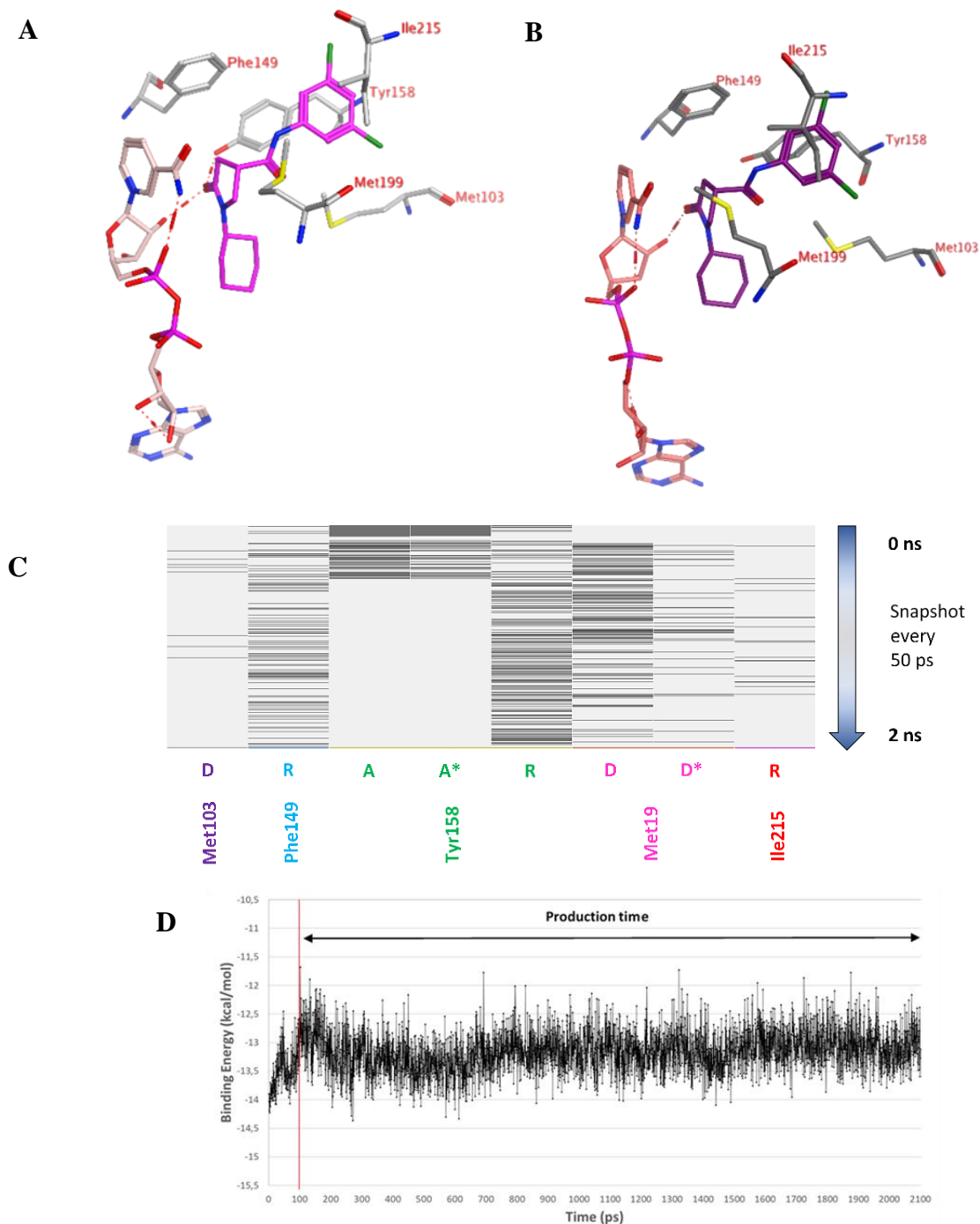


Figure 2. (A) The MtnhA (4TZK)-reference ligand (indicated purple) ($t = 0$ ns). NAD^+ is presented as a cofactor (pink). (B) The MtnhA (4TZK)-reference ligand after a 2 ns MD simulation. (C) The protein-ligand interaction fingerprint (PLIF) showing the interaction of reference ligand with the MtnhA (4TZK) binding pocket residues during the simulation as barcodes (a black line indicating the presence of the interaction at snapshot). (D) The binding energy (kJ/mol) between reference ligand and MtnhA (4TZK). Hydrogen bonds are indicated in red dashed lines. “D” indicates side chain donor interactions, “R” indicates H-arene interactions and “A” indicates sidechain acceptor interactions. Two interactions of the same type per residue (for example “A” for Tyr158) indicate that multiple interactions of the specified type between ligand and residue are formed. “*” indicates the strong interactions. The arrow indicates the sequence of snapshots of every 50 ps from 0 to 2 ns.

In docking studies, the carboxyl moiety at the thiazolidinone ring of the reference ligand form hydrogen bonds with NAD⁺ and sidechain of Tyr158. Phenyl ring may form hydrophobic interactions or H-arene with the sidechains of Tyr158 and Ile215 (Figure 2A).

In MD simulation, by using the protein-ligand interaction fingerprint (PLIF) tool of MOE (v2019.01.02, Chemical Computing Group Inc., Montreal, Quebec, Canada), the intermolecular interactions between the enzyme active site and reference ligand were analyzed (Figure 2C). The formed main interactions during the 2 ns simulation (represented as 40 snapshots; one snapshot per 50 ps) were with Met103 (“D”: side chain donor interaction), Phe149 (“R”: H-Arene interaction), Tyr158 (“A”: side chain acceptor interaction and “R”), Met199 (“D”) and Ile215 (“R”). The hydrogen bond between the reference ligand and the sidechain of Tyr158 was observed in 39% of the snapshots. Another formed hydrogen bond between the reference ligand and the sidechain of Met199 was observed in 31% of the frames, including the first (0 ns) and the last (2 ns). Interaction between reference ligand and NAD⁺ with the distance smaller than 3.2 Å accepted as moderate,⁴² as shown in Figure 2C, this interaction is observed in 100% of the production run snapshots. The hydrogen bond between the lactam carbonyl group of the reference ligand and the hydroxyl group at the furan ring of the NAD⁺ seems to be stable during MD simulation. (Figure 2B). The calculated average binding energy between reference ligand and MtlInhA (4TZK) was -13.1 kJ/mol with the root-mean-square deviation value (RMSD) of 0.3614 Å (Figure 2D).

Compounds **3-16** have been docked into the active site of the MtlInhA (4TZK) crystal structure. Interactions between MtlInhA (4TZK) active site and compound **7**, which has the best inhibition ratio against *M. Tuberculosis* strain H37Rv (98%) is shown in Figure 3A. Hydroxyl group of the ligand forms a hydrogen bond with cofactor NAD⁺ and another hydrogen bond between amide functionality of the ligand and the backbone of the Gly96 is observed.

During a 2 ns MD simulation (represented as 40 snapshots; one snapshot per 50 ps), the observed main interactions between ligands and active site were Gly96 (“d”: backbone donor interaction, “a”: backbone acceptor interaction and “R”: H-Arene interaction), Phe97 and Met98 (both “a”), Met103 (“D”: side chain donor interaction), Phe149 (“R”) and Met199 (“D”, “a” and “R”) as shown in Figure 3C. The hydrogen bond between the ligand and the backbone of Gly96 was observed in 99% of the snapshots. Another formed hydrogen bond between the ligand and the backbone of Met98 was observed in 63% of the frames, including the first (0 ns) and the last (2 ns). In addition, a hydrogen bond formed by sidechain of Met103 is observed in 44% of the snapshots. Although not shown in Figure 3C, the interaction between the ligand and NAD⁺ (in a smaller distance than 3.2 Å) is observed in 74.4 % of the production run snapshots. Therefore, the interaction between oxygen atom (O1A) of the phosphate group at NAD⁺ and amide nitrogen atom of the ligand may be kept. (Figure 3B). The calculated average binding energy between compound **7** and MtlInhA (4TZK) was -12.9 kJ/mol (RMSD: 0.3642 Å) (Figure 3D).

3.3.2. Docking Studies and MD Simulations into the Active Site of MtlInhA(4BQP)

With the same purpose above, docking studies and a 2 ns MD simulation was performed on the MtlInhA (4BQP) crystal structure in complex with the methyl-thiazole compound as reference ligand, and NAD⁺ (Nicotinamide Adenine Dinucleotide) is presented as a cofactor (pink) of the enzyme (Figure 4).

In docking studies, it is observed that the reference ligand interacts with NAD⁺ and forms a hydrogen bond with the backbone of Met98. Dichloro-phenyl ring of the ligand located at a hydrophobic pocket and may interact with Tyr158 and Ile202 backbones (Figure 4A).

The main detected interactions during 2 ns the simulation (represented as 40 snapshots; one snapshot per 50 ps) were with Gln103 (“D”: sidechain donor interaction), Met103 (“R”: H-Arene interaction), Ala198 (“d”: backbone donor interaction) and Ile202 (“R”), analyzed with PLIF tool of MOE (Figure 4C). The hydrogen bond between reference ligand and the sidechains of Met103 and Ala198 were observed in 39% and 30% of the snapshots, respectively. Although not shown in Figure 4C, three different interactions between the ligand and NAD⁺ are detected during the MD simulation, again in a smaller distance than 3.2 Å.

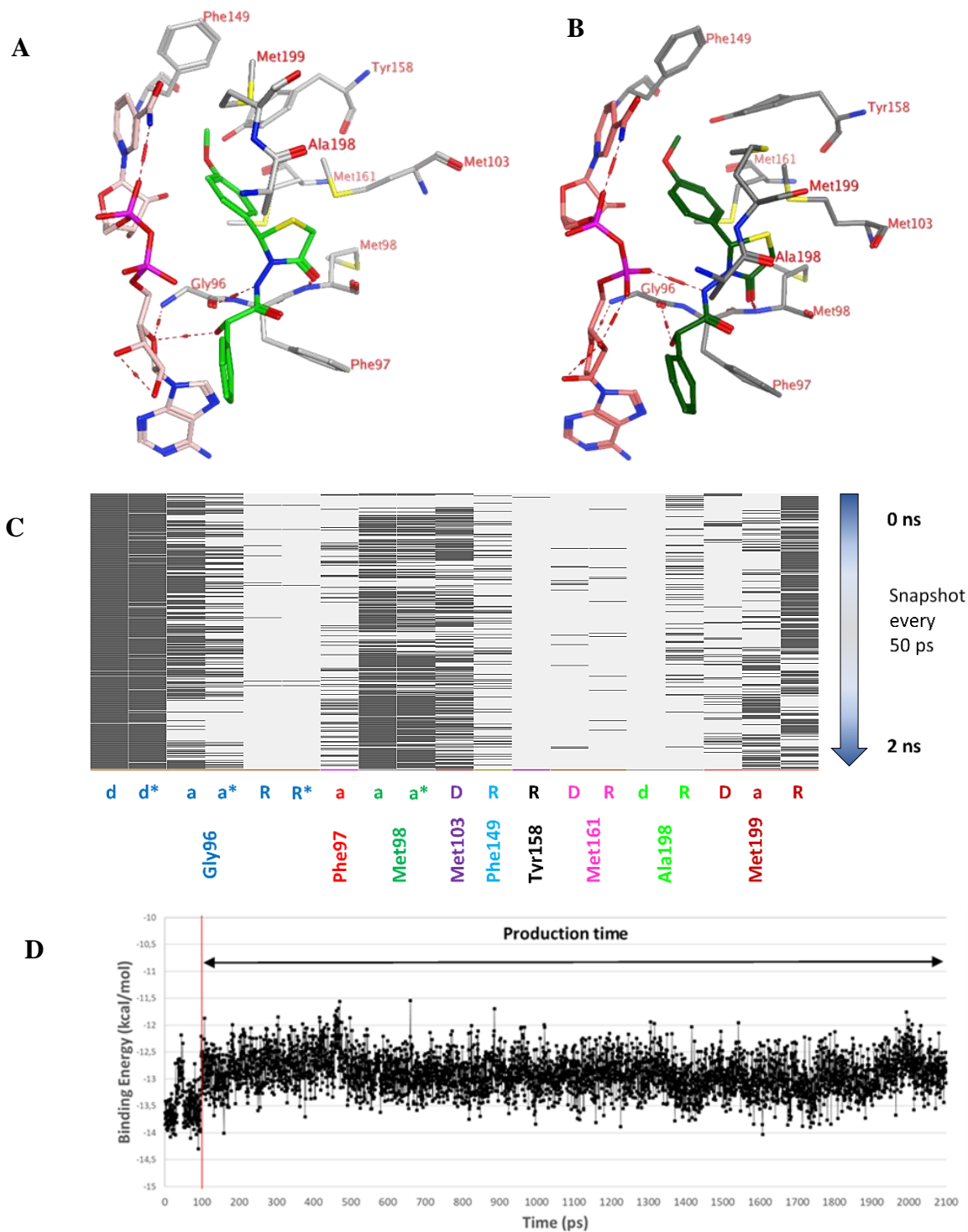


Figure 3. (A) The MtInhA (4TZK)-compound 7 (green) obtained from docking ($t = 0$ ns). NAD^+ is presented as a cofactor (pink). (B) The MtInhA (4TZK)-compound 7 after a 2 ns MD simulation. (C) The protein-ligand interaction fingerprint (PLIF) showing the interaction of reference ligand with the MtInhA (4TZK) binding pocket residues during the simulation as barcodes (a black line indicating the presence of the interaction at snapshot). (D) The binding energy (kJ/mol) between reference ligand and MtInhA (4TZK). “d” indicates backbone donor interactions, “a” indicates backbone acceptor interactions, “R” indicates H–arene interactions and “D” indicates side chain donor interactions. Two interactions of the same type per residue (for example “R” for Gly96) indicate that multiple interactions of the specified type between ligand and residue are formed. “*” indicates the strong interactions. The arrow indicates the sequence of snapshots of every 50 ps from 0 to 2 ns.

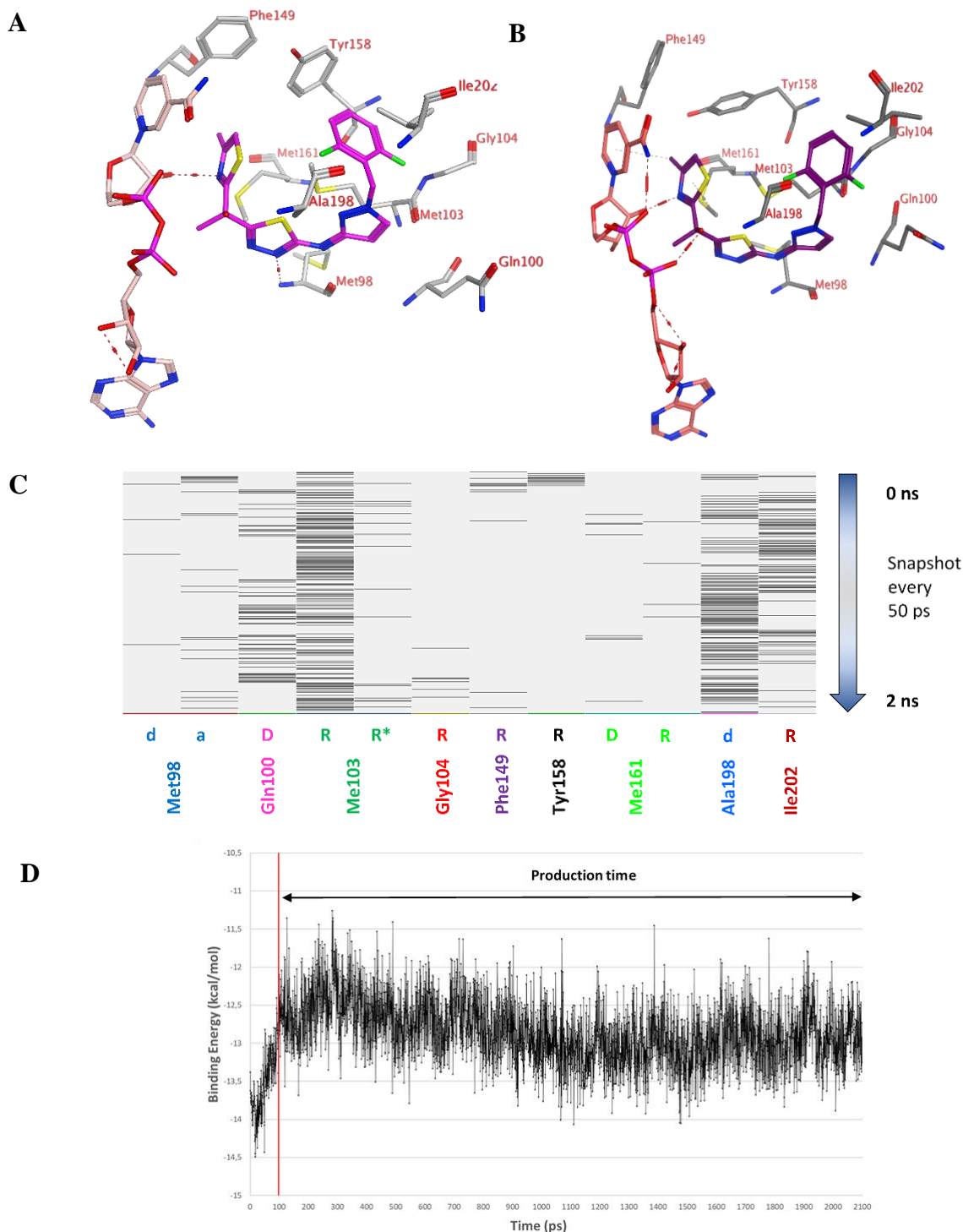


Figure 4. (A) The MtInhA (4BQP)-reference ligand (indicated with purple) ($t = 0$ ns). NAD^+ is presented as a cofactor (pink). (B) The MtInhA (4BQP)-reference ligand after a 2 ns MD simulation. (C) The protein-ligand interaction fingerprint (PLIF) showing the interaction of reference ligand with the MtInhA (4BQP) binding pocket residues during the simulation as barcodes (a black line indicating the presence of the interaction at snapshot). (D) The binding energy (kJ/mol) between reference ligand and MtInhA (4BQP). “d” indicates backbone donor interactions, “a” indicates backbone acceptor interactions, “D” indicates side chain donor interactions, and “R” indicates H–arene interactions. Two interactions of the same type per residue (for example “R” for Met103) indicate that multiple interactions of the specified type between ligand and residue are formed. “*” indicates the strong interactions. The arrow indicates the sequence of snapshots of every 50 ps from 0 to 2 ns.

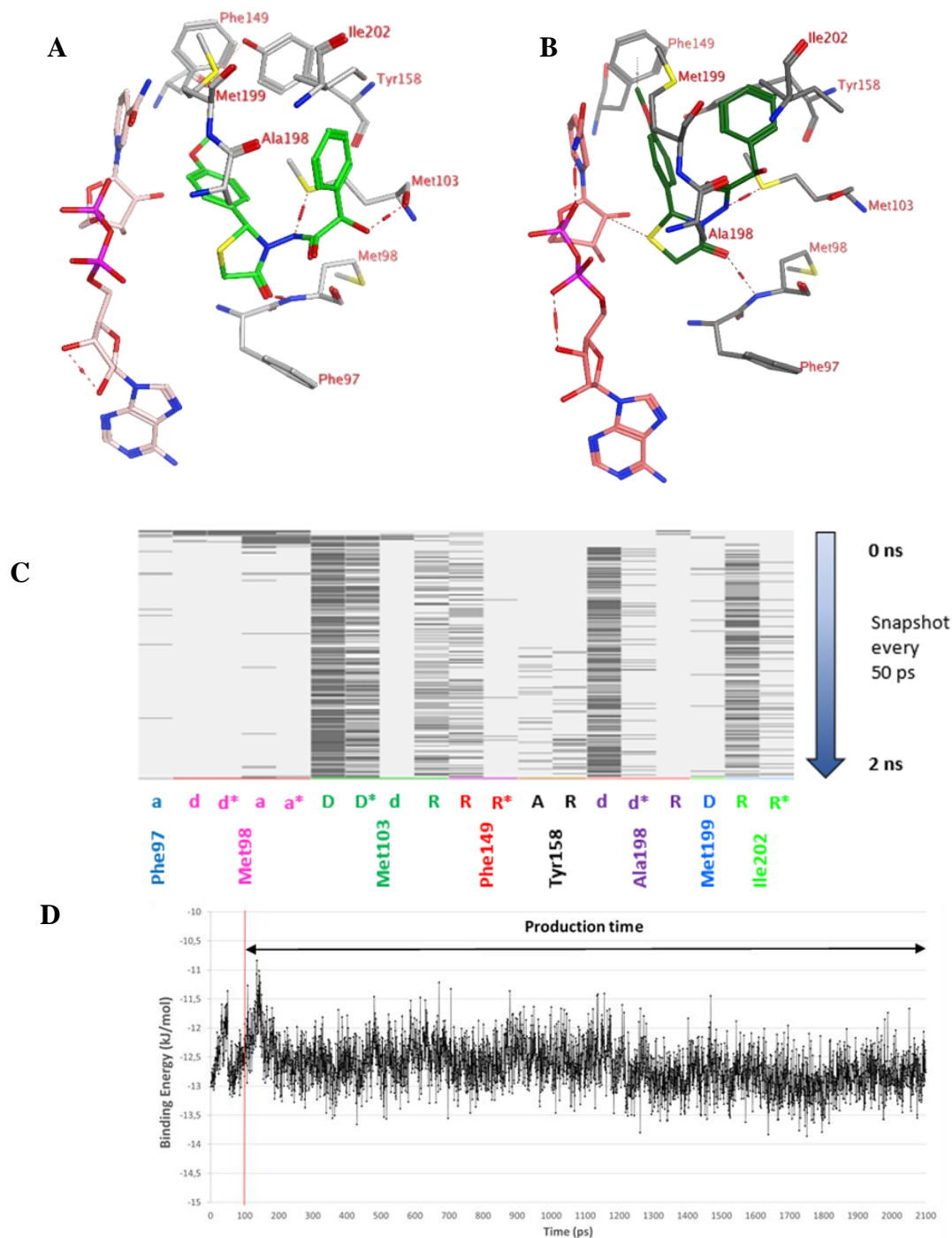


Figure 5. (A) The MtInhA (4BQP)-compound 7 (green) obtained from docking ($t = 0$ ns). NAD^+ is presented as a cofactor (pink). (B) The MtInhA (4BQP)-compound 7 after a 2 ns MD simulation. (C) The protein-ligand interaction fingerprint (PLIF) showing the interaction of reference ligand with the MtInhA (4BQP) binding pocket residues during the simulation as barcodes (a black line indicating the presence of the interaction at snapshot). (D). The binding energy (kJ/mol) between ligand and MtInhA (4BQP). “a” indicates backbone acceptor interactions, “d” indicates backbone donor interactions, “D” indicates sidechain donor interactions, and “R” indicates H-arene interactions, “A” indicates sidechain acceptor interactions. Two interactions of the same type per residue (for example “D” for Met103) indicate that multiple interactions of the specified type between ligand and residue are formed. “*” indicates the strong interactions. The arrow indicates the sequence of snapshots of every 50 ps from 0 to 2 ns.

A hydrogen bond between thiaziazole nitrogen of the reference ligand and the hydroxyl group of NAD⁺ observed in 96.4% of the production run snapshots. The hydroxyl group of the ligand may form two interactions but not the same time with oxygen atoms O1N and O1A of the phosphate groups at NAD⁺. The interactions were observed in 88.4% and 92.1% of all frames during 2 ns MD simulation, respectively (Figure 4B). It can be said that compound **7** may interact in general with NAD⁺ in three ways. The calculated average binding energy between reference ligand and MtInhA (4BQP) was -12.87 kJ/mol (RMSD: 0.4323 Å) (Figure 4D).

Fourteen newly synthesized thiazolidinones (i.e., compounds **3-16**) have been docked into the active site of the MtInhA (4BQP) crystal structure. Compound **7**, as shown in Figure 5A, forms a strong a hydrogen bond through its hydroxyl group with the backbone of Met103. Another hydrogen bond between the sidechain of Met103 and the amide group of the ligand is observed. The carbonyl functionality of the thiazolidinone ring interacts with both Met198 and Phe97 by hydrogen bonds. 4-OCH₃ substituted phenyl may form hydrophobic interactions with sidechain of Phe149 and Tyr158, while 4-OCH₃ moiety may also form H-arene interactions with only Phe149 side chain.

In MD simulation of compound **7** (represented as 40 snapshots; one snapshot per 50 ps), the detected main interactions between ligand and active site were Met103 (“D”: sidechain donor interaction and “d”: side chain acceptor interaction), Phe 149 (“R”: H-Arene interaction), Ala198 (“D”) and Ile202 (“R”). The H-arene interaction between the ligand and the sidechain of Ile202 was observed in 48% of the frames, including the first (0 ns) and the last (2 ns). The hydrogen bond between the ligand and the sidechain of Met103 was observed in 79% of the snapshots. Another formed hydrogen bond between the ligand and the backbone of Ala198 was observed in 63% of the frames, including the first (0 ns) and the last (2 ns). In addition, an H-arene interaction formed by sidechain of Ile202 is observed in 48% of the snapshots. Although not shown in Figure 5B, the interaction between the methoxy group of compound **7** and the hydroxyl group of NAD⁺ is observed in 2.2 % of the production run snapshots. As a result of the steric barrier of methyl, it may not possibly form a strong stable hydrogen bond between the ligand and NAD⁺ (Figure 5B). The calculated average binding energy between compound **7** and MtInhA (4BQP) was -12.6 kJ/mol (RMSD: 0,3879 Å) (Figure 5D).

As noted above, the docking studies suggest that the new compounds interact with the targeted enzymes MtInhA (4TZK) and (4BQP) like their reference ligands. According to the MD simulations, the binding energies of compound **7** is similar to the reference ligands. Therefore, it may be expected that compound **7** could show its antimycobacterial action through inhibiting both the targeted MtInhA enzymes.

4. Conclusion

In the present work, fourteen new 2-hydroxy-*N*-(4-oxo-2-substitutedphenyl-1,3-thiazolidin-3-yl)-2-phenylacetamide derivatives were screened with *in-vitro* tests for their antimycobacterial activity against the pathogenic bacterium *M. tuberculosis* strain H37Rv. Compound **7** with a methoxy group at the para position of the phenyl ring exhibited the highest inhibition (98%). In order to explain antimycobacterial action of the fourteen compounds, inhibition of the MtInhA enzymes (4TZK, 4BQP and 4BGE) were investigated with docking and dynamic simulations, as potential promising targets. For all MtInhA enzymes, all compounds were able to interact with the active sites in similar but not exactly the same ways with reference ligands. Compound **7**, one of the top-ranked molecules in molecular modelling studies, showed strong interactions with the targeted enzymes and suggested as an inhibitor of MtInhA. Collectively, it is indicated that the inhibition of the MtInhA could be a part of the antimycobacterial activity of the new compounds and further development of these derivatives may present strong candidates for the treatment of tuberculosis.

Acknowledgments

Antimycobacterial data were provided by the Tuberculosis Antimicrobial Acquisition and Coordinating Facility (TAACF) through a research and development contract with the U.S. National Institute of Allergy and Infectious Diseases. Dr. Joseph A. Maddry (TAACF) and his team are recognized for their collaboration. This work was supported by the Research Fund of Istanbul University (Project number: 178/15012004).

Supporting Information

Supporting information accompanies this paper on <http://www.acgpubs.org/journal/organic-communications>.

ORCID

Özlen Güzel-Akdemir: [0000-0003-3680-1945](https://orcid.org/0000-0003-3680-1945)

Kübra Demir-Yazıcı: [0000-0001-9928-4733](https://orcid.org/0000-0001-9928-4733)

Muhammed Trawally: [0000-0002-0041-4612](https://orcid.org/0000-0002-0041-4612)

Serap İpek Dingiş-Birgül: [0000-0003-2242-4296](https://orcid.org/0000-0003-2242-4296)

Atilla Akdemir: [0000-0001-8416-0471](https://orcid.org/0000-0001-8416-0471)

References

- [1] Smith, I. *Mycobacterium tuberculosis* pathogenesis and molecular determinants of virulence. *Clin Microbiol Rev.* **2003**, *16*(3), 463-496.
- [2] World Health Organization. Tuberculosis Homepage. available online: <https://www.who.int/news-room/fact-sheets/detail/tuberculosis> (accessed on 5 May 2020)
- [3] World Health Organization. *Global tuberculosis reports.* **2019**, *23*, 1-4.
- [4] World Health Organization. Tuberculosis Fact Sheets. Available online: <https://www.who.int/news-room/fact-sheets/detail/tuberculosis> (accessed on 5 May 2020).
- [5] Glaziou, P. Predicted impact of the COVID-19 pandemic on global tuberculosis deaths in 2020. *medRxiv.* **2020**, *5*, 1-7.
- [6] Zhang, Y.; Post-Martens, K.; Denkin, S. New drug candidates and therapeutic targets for tuberculosis therapy. *Drug Discovery Today.* **2006**, *11*, 21–27.
- [7] Chan, E. D. Current medical treatment for tuberculosis. *BMJ.* **2002**, *325*(7375), 1282–1286.
- [8] Gygli, S. M.; Borrell, S.; Trauner, A.; Gagneux, S. Antimicrobial resistance in *Mycobacterium tuberculosis*: mechanistic and evolutionary perspectives. *FEMS Microbiol. Rev.* **2017**, *011*, 354–373.
- [9] Kanetaka, H.; Koseki, Y.; Taira, J.; Umei, T.; Komatsu, H.; Sakamoto, H.; Gulen, G.; Sacchetti, J. C.; Kitamura, M.; Aoki, S. Discovery of InhA inhibitors with anti-mycobacterial activity through a matched molecular pair approach. *Eur. J. Med. Chem.* **2015**, *94*, 378–385.
- [10] Duan, X.; Xiang, X.; Xie, J. Crucial components of mycobacterium type II fatty acid biosynthesis (Fas-II) and their inhibitors. *FEMS Microbiol. Lett.* **2014**, *360* (2), 87–99.
- [11] Quémard, A.; Sacchetti, J. C.; Dessen, A.; Vilcheze, C.; Bittman, R.; Jacobs, W. R.; Blanchard, J. S. Enzymatic Characterization of the target for isoniazid in *Mycobacterium tuberculosis*. *Biochemistry* **1995**, *34* (26), 8235–8241.
- [12] Vigorita, M. G.; Ottanà, R.; Monforte, F.; Maccari, R.; Trovato, A.; Monforte, M. T.; Taviano, M. F. Synthesis and antiinflammatory, analgesic activity of 3,3'-(1,2-ethanediyl)-bis[2-aryl-4-thiazolidinone] chiral compounds. *Bioorg. Med. Chem. Lett.* **2001**, *11* (21), 2791–2794.
- [13] Vicini, P.; Geronikaki, A.; Anastasia, K.; Incerti, M.; Zani, F. Synthesis and antimicrobial activity of novel 2-thiazolylimino-5-arylidene-4-thiazolidinones. *Bioorganic Med. Chem.* **2006**, *14* (11), 3859–3864.
- [14] D'Ascenzio, M.; Bizzarri, B.; De Monte, C.; Carradori, S.; Bolasco, A.; Secci, D.; Rivanera, D.; Faulhaber, N.; Bordón, C.; Jones-Brando, L. Design, Synthesis and biological characterization of thiazolidin-4-one derivatives as promising inhibitors of *Toxoplasma gondii*. *Eur. J. Med. Chem.* **2014**, *86*, 17–30.
- [15] Sonam; Chahal, V.; Kakkar, R. Theoretical study of the structural features and antioxidant potential of 4-thiazolidinones. *Struct. Chem.* **2020**, 1–10.
- [16] Mishchenko, M.; Shtrygol, S.; Kaminsky, D.; Lesyk, R. Thiazole-bearing 4-thiazolidinones as new anticonvulsant agents. *Sci. Pharm.* **2020**, *88* (1), 16.
- [17] Suryawanshi, R.; Jadhav, S.; Makwana, N.; Desai, D.; Chaturbhuj, D.; Sonawani, A.; Idicula-Thomas, S.; Murugesan, V.; Katti, S. B.; Tripathy, S.; et al. Evaluation of 4-thiazolidinone derivatives as potential reverse transcriptase inhibitors against HIV-1 drug resistant strains. *Bioorg. Chem.* **2017**, *71*, 211–218.
- [18] De Monte, C.; Carradori, S.; Bizzarri, B.; Bolasco, A.; Caprara, F.; Mollica, A.; Rivanera, D.; Mari, E.; Zicari, A.; Akdemir, A.; et al. Anti-candida activity and cytotoxicity of a large library of new N-substituted-1,3-Tthiazolidin-4-one derivatives. *Eur. J. Med. Chem.* **2016**, *107*, 82–96.

- [19] Türe, A.; Ergül, M.; Ergül, M.; Altun, A.; Küçükgül, İ. Design, synthesis, and anticancer activity of novel 4-thiazolidinone-phenylaminopyrimidine hybrids. *Mol. Divers.* **2020**, *1*, 3.
- [20] Küçükgül, Ş. G.; Oruç, E. E.; Rollas, S.; Şahin, F.; Özbek, A. Synthesis, characterisation and biological activity of novel 4-thiazolidinones, 1,3,4-oxadiazoles and some related compounds. *Eur. J. Med. Chem.* **2002**, *37* (3), 197–206.
- [21] Babaoglu, K.; Page, M. A.; Jones, V. C.; McNeil, M. R.; Dong, C.; Naismith, J. H.; Lee, R. E. Novel inhibitors of an emerging target in *Mycobacterium tuberculosis*; substituted thiazolidinones as inhibitors of DTDP-rhamnose synthesis. *Bioorganic Med. Chem. Lett.* **2003**, *13* (19), 3227–3230.
- [22] Güzel-Akdemir, Ö.; Angeli, A.; Demir, K.; Supuran, C. T.; Akdemir, A. Novel thiazolidinone-containing compounds, without the well-known sulphonamide zinc-binding group acting as human carbonic anhydrase IX inhibitors. *J. Enzyme Inhib. Med. Chem.* **2018**, *33* (1), 1299–1308.
- [23] Güzel-Akdemir, Ö.; Carradori, S.; Grande, R.; Demir-Yazıcı, K.; Angeli, A.; Supuran, C. T.; Akdemir, A. Development of thiazolidinones as fungal carbonic anhydrase inhibitors. *Int. J. Mol. Sci.* **2020**, *21* (8), 2960.
- [24] Zieliński, W.; Kudelko, A.; Czardybon, W. The synthesis of 4-acylamino-1,2,4-triazole derivatives in the reaction of α -hydroxyacid hydrazides and orthoesters. *J. Heterocycl. Chem.* **2005**, *42* (7), 1393–1397.
- [25] Inderlied, C. B. Antimycobacterial susceptibility testing: present practices and future trends. *Eur. J. Clin. Microbiol. Infect. Dis.* **1994**, 980–993.
- [26] Demir-Yazıcı, K.; Güzel-Akdemir, Ö.; Angeli, A.; Supuran, C. T.; Akdemir, A. Novel indole-based hydrazones as potent inhibitors of the α -class carbonic anhydrase from pathogenic bacterium *Vibrio cholerae*. *Int. J. Mol. Sci.* **2020**, *21* (9), 3131.
- [27] Halgren, T. A. Merck molecular force field. I. basis, form, scope, parameterization, and performance of MMFF94. *J. Comput. Chem.* **1996**, *17* (5–6), 490–519.
- [28] Labute, P. Protonate3D: Assignment of ionization states and hydrogen coordinates to macromolecular structures. *Proteins Struct. Funct. Bioinforma.* **2009**, *75* (1), 187–205.
- [29] Case, D.A.; Babin, V.; Berryman, J.T., Betz, R.M.; Cai, Q.; Cerutti, D.S.; Cheatham, T.E. III. Darden, T.A.; Duke, R.E.; Gohlke, H.; Goetz, A.W.; Gusarov, S.; Homeyer, N.; Janowski, P.; Kaus, J.; Kolossváry, I.; Kovalenko, A.; Lee, T.S.; LeGrand, S.; Luchko, T.; Luo, R.; Madej, B.; Merz, K.M.; Paesani, F.; Roe, D.R.; Roitberg, A.; Sagui, C.; Salomon-Ferrer, R.; Seabra, G.; Simmerling, C.L.; Smith, W.; Swails, J.; Walker, R.C.; Wang, J.; Wolf, R.M.; Wu, X.; Kollman P. *AMBER 14*, (University of California, San Francisco) **2014**, 1–814.
- [30] Labute, P. The Generalized born/volume integral implicit solvent model: estimation of the free energy of hydration using London dispersion instead of atomic surface area. *J. Comput. Chem.* **2008**, *29* (10), 1693–1698.
- [31] Phillips, J. C.; Braun, R.; Wang, W.; Gumbart, J.; Tajkhorshid, E.; Villa, E.; Chipot, C.; Skeel, R. D.; Kalé, L.; Schulten, K. Scalable molecular dynamics with NAMD. *J. Comput. Chem.* **2005**, *33*(1), 1781–1802.
- [32] Taylor, P. J. The infra-red spectroscopy of some 2-substituted thiazolid-4-ones, a new class of enamino-ketone-II. infra-red assignments and chemical implications. *Spectrochim. Acta Part A Mol. Spectrosc.* **1970**, *26* (1), 165–194.
- [33] Kaynak, F. B.; Öztürk, D.; Özbey, S.; Çapan, G. New N'-alkylidene/cycloalkylidene derivatives of 5-methyl-3-phenyl-1H-indole-2-carbohydrazide: synthesis, crystal structure, and quantum mechanical calculations. *J. Mol. Struct.* **2005**, *740* (1–3), 213–221.
- [34] Güzel, Ö.; İlhan, E.; Salman, A. Synthesis and antimycobacterial activity of new 2-hydroxy-N-(3-oxo-1-thia-4-azaspiro[4.4]non-4-yl)/(3-oxo-1-thia-4-azaspiro[4.5]dec-4-yl)-2, 2-diphenylacetamide derivatives. *Monatsh Chem.* **2006**, *137* (6), 795–801.
- [35] Verma, A.; Saraf, S. K. 4-Thiazolidinone - a biologically active scaffold. *Eur. J. Med. Chem.* **2008**, *43*(5), 897–905.
- [36] Gupta, A.; Singh, R.; Sonar, P. K.; Saraf, S. K. Novel 4-thiazolidinone derivatives as anti-infective agents: synthesis, characterization, and antimicrobial evaluation. *Biochem. Res. Int.* **2016**, *2016*, 1–8.
- [37] Ergenç, N.; Çapan, G.; Günay, N. S.; Özkirimli, S.; Güngör, M.; Özbey, S.; Kendi, E. Synthesis and hypnotic activity of new 4-thiazolidinone and 2-thioxo-4,5-imidazolidinedione derivatives. *Arch. Pharm. (Weinheim)*. **1999**, *332* (10), 343–347.
- [38] Karali, N.; İlhan, E.; Gürsoy, A.; Kiraz, M. New cyclohexylidenehydrazide and 4-aza-1-thiaspiro[4.5]decan-3-one derivatives of 3-phenyl-4 (3H)-quinazolinones. *Farmaco* **1998**, *53* (5), 346–349.
- [39] He, X.; Alian, A.; Stroud, R.; Ortiz De Montellano, P. R. Pyrrolidine carboxamides as a novel Class of inhibitors of enoyl acyl carrier protein reductase from *Mycobacterium tuberculosis*. *J. Med. Chem.* **2006**, *49* (21), 6308–6323.
- [40] Vilchèze, C.; Wang, F.; Arai, M.; Hazbón, M. H.; Colangeli, R.; Kremer, L.; Weisbrod, T. R.; Alland, D.; Sacchettini, J. C.; Jacobs, W. R. Transfer of a point mutation in *Mycobacterium tuberculosis* InhA resolves the target of isoniazid. *Nat. Med.* **2006**, *12* (9), 1027–1029.

- [41] Dessen, A.; Quémard, A.; Blanchard, J. S.; Jacobs, W. R.; Sacchetti, J. C. Crystal structure and function of the isoniazid target of *Mycobacterium tuberculosis*. *Science* (80-.). **1995**, 267 (5204), 1638–1641.
- [42] Jeffrey, George A.; *An introduction to hydrogen bonding*, Oxford University Press, *New York*, 1997.

A C G
publications

© 2020 ACG Publications